Towards Design and Control of Soft Robotic Systems

Brandon Jonathan Caasenbrood

About the cover **Explanation**

Photo: ??



The work described in this thesis was carried out at the Eindhoven University of Technology (TU/e).

A catalogue record is available from the Eindhoven University of Technology Library. ISBN: ??

Typeset with LaTeX. Cover design by ?? Reproduction by ??

FSC keurmerk hier

© 2021 by ??. All rights reserved.

Towards Design and Control of Soft Robotic Systems

PROEFSCHRIFT

ter verkrijging van de graad van doctor aan de Technische Universiteit Eindhoven, op gezag van de rector magnificus prof.dr.ir. F.P.T. Baaijens, voor een commissie aangewezen door het College voor Promoties, in het openbaar te verdedigen op 21 December 2022 om 16.00 uur

door

Brandon Jonathan Caasenbrood geboren te Roermond Dit proefschrift is goedgekeurd door de promotoren en de samenstelling van de promotiecommissie is als volgt:

voorzitter: ??

1º promotor: ??

2º promotor: ??

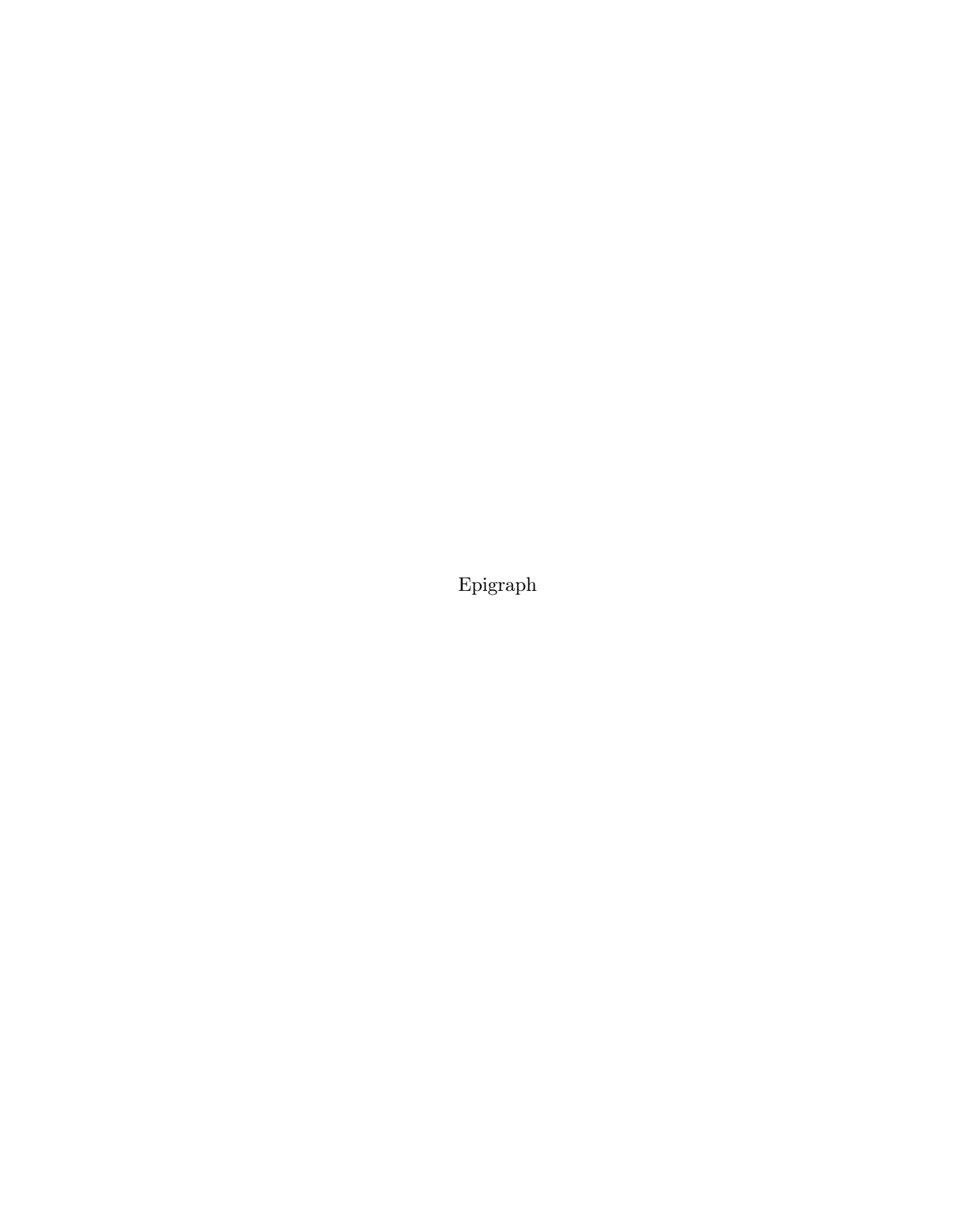
leden: ??

??

??

adviseur: ??

Het onderzoek dat in dit proefschrift wordt beschreven is uitgevoerd in overeenstemming met de ${\rm TU/e}$ Gedragscode Wetenschapsbeoefening.



Summary

Towards Design and Control of Soft Robotic Systems

Hello, here is some text without a meaning. This text should show what a printed text will look like at this place. If you read this text, you will get no information. Really? Is there no information? Is there a difference between this text and some nonsense like "Huardest gefburn"? Kjift – not at all! A blind text like this gives you information about the selected font, how the letters are written and an impression of the look. This text should contain all letters of the alphabet and it should be written in of the original language. There is no need for special content, but the length of words should match the language.

Contents

Sι	ımm	ary	j			
1	Modeling of Continuum Soft Robots – Piece-wise Constant case					
	1.1	Design and fabrication	2			
	1.2	Continuum dynamic model	3			
	1.3	Extension to multi-link dynamics	9			
	1.4	Efficient computation of the continuum dynamics	11			

iv Contents

Modeling of Continuum Soft Robots – Piece-wise Constant case

The motion complexity and use of exotic materials in soft robotics call for accurate and computationally efficient models intended for control. To reduce the gap between material and control-oriented research, we build upon the existing Piecewise-Constant Curvature framework by incorporating hyper-elastic and visco-elastic material behavior. In this work, the continuum dynamics of the soft robot are derived through the differential geometry of spatial curves, which are then related to Finite-Element data to capture the intrinsic geometric and material nonlinearities. To enable fast simulations, a reduced-order integration scheme is introduced to compute the dynamic Lagrangian matrices efficiently, which in turn allows for real-time (multi-link) models with sufficient numerical precision. By exploring the passivity and using the parametrization of the hyper-elastic model, we propose a passivity-based adaptive controller that enhances robustness towards material uncertainty and unmodeled dynamics – slowly improving their estimates online. As a study case, a fully 3D-printed soft robot manipulator is developed, which shows good correspondence with the dynamic model under various conditions, e.g., natural oscillations, forced inputs, and under tip-loads. The solidity of the approach is demonstrated through extensive simulations, numerical benchmarks, and experimental validations.

This chapter is based on:

Caasenbrood, B. J., Pogromsky, A. Y., and Nijmeijer, H. (2020). Dynamic modeling of hyper-elastic soft robots using spatial curves. IFAC-PapersOnLine, 53, 9238–9243.

^{2.} Caasenbrood, B. J., Pogromsky, A. Y., and Nijmeijer, H. (2021). **Dynamic Modeling of Hyper-elastic Soft Robots through Differential Geometry of Curves** Soft Robotics, 2021. (under review).

1.1 Design and fabrication

By using additive manufacturing, we developed a soft and flexible robot manipulator that is suitable for pick-and-place application. The 3-DOF soft robot can be seen in Figure ??. The soft robot manipulator in this work is loosely inspired by the elephant whose trunk-appendage consist mainly of parallel muscles without skeletal support. The anatomy of elephant's trunk provides an excellent study case, as they naturally exhibit continuum-body bending and moderate elongation [?,?,?]. Similar to the earlier soft robotic designs [?,?], the developed soft robot can undergo three-dimensional movement by inflation or deflation of embedded pneumatic bellow network. The soft robot can achieve bending in any preferred direction by differential pressurization of each channel (<0.1 MPa). Whereas, simultaneous pressurization accomplishes moderate elongation.

The soft robot is exclusively composed of a printable, flexible thermoplastic elastomer (Young's modulus \leq 80 MPa), which intrinsically promotes softness and dexterity. The elastomer material is developed explicitly for Selective Laser Sintering (SLS), a 3-Dimensional (3D) printing method that uses a laser to solidify powdered material. The main advantage of SLS printing over other techniques is that the printed parts are fully self-supported, which allows for complex and highly detailed structures. It should be mentioned that the layer-by-layer material deposition will introduce undesired anisotropic mechanical effects. To mitigate anisotropy, the bellows are printed orthogonal to the printing plane, thereby ensuring mechanical symmetry. For the majority of this work, the 3D-printed soft robot in Figure ?? will form the basis of the dynamical model. The 3D-model is made available at the open repository [?].

1.2 Continuum dynamic model

As mentioned previously, soft robots are composed of soft bodies that may be regarded as a continuum body with (theoretically) infinitely many degrees-of-freedom (DOF). In this section, we aim to derive a compact and computationally efficient model that envelops the continuous dynamics of a soft robot through a small set of generalized coordinates $\mathbf{q} \in \mathcal{Q}$ and their respective generalized velocities $\dot{\mathbf{q}}(t) \in \mathbb{R}^n$ with n the number of active joint variables. We base the modeling framework on the work of Mochiyama et al. [?] who outlined a theoretical foundation for continuum manipulators. Their work is extended upon by including extensibility, serial-chaining of multiple soft-links, pneumatic actuation, and the introduction of nonlinear and time-dependent material behavior. Earlier modeling strategies addressing similar issues can be found in from Godage et al. [?,?], Della Santina et al. [?,?,?], Renda et al. [?], and Boyer et al. [?]. Leveraging from the aforementioned works, the continuous dynamics of a soft robot manipulator can be written in the familiar Lagrangian form:

$$M(q)\ddot{q} + h(q,\dot{q}) = Q^{\text{nc}}, \tag{1.1}$$

where $M(q) \in \mathbb{R}^{n \times n}$ denotes the generalized inertia matrix, $h(q, \dot{q}) \in \mathbb{R}^n$ a vector of nonlinear state-dependent force contributions. In this work, a similar modeling framework is adopted; however, we propose an extension to incorporate FEM-driven data to more accurately reflect the underlying continuum mechanics – in particular hyper-elasticity; and we propose a numerical scheme that allows for fast computation of the continuous dynamics. For completeness, we will recapitulate on the modeling approach here.

1.2.1 Kinematics of elastic continuum bodies

To represent the hyper-flexible configuration of the soft robot, let us consider a smooth spatial curve that passes through the geometric center of the continuously deformable body, as shown in Figure ??. In literature, this curve is called the 'backbone curve' as it simplifies the three-dimensional deformation imposed by distributed forces acting on the elastic body. The arc-length of the backbone corresponds to the extensible length of the soft robot denoted by the variable $l(t) \in [l_-, l_+]$ which we assume bounded $l_+ \geq l \geq l_-$, and let L be a constant denoting the total unstressed length of the soft robot. Next, let us introduce a spatial variable $\sigma \in \mathbb{X}$ that belongs to the one-dimensional material domain of the backbone curve, i.e., $\mathbb{X} = [0, L]$. Let it be clear that the spatial variable σ represents the arc-length of a material coordinate along the undeformed material domain of the soft robot manipulator.

Given each material coordinate, we wish to find a suitable low-dimensional joint representation q(t) such that the position vector ${}^{0}p$ anywhere on the con-

tinuous backbone can be written as a mapping from generalized coordinates and space into \mathbb{R}^3 :

$${}^{0}\boldsymbol{p}: \mathbb{X} \times \mathcal{Q}(t) \to \mathbb{R}^{3};$$
 (1.2)

and similarly the rotation matrix ${}^{0}\Phi(\sigma, \mathbf{q})$ by a mapping from the generalized coordinates and space into SO(3):

$${}^{0}\mathbf{\Phi}: \mathbb{X} \times \mathcal{Q}(t) \to \mathrm{SO}(3),$$
 (1.3)

where SO(3) denotes the special orthogonal group for rotations about the origin of \mathbb{R}^3 , and $n=\dim(\boldsymbol{q})$ the state dimension. Under this notion, the position vectors ${}^0p(q,0)$ and ${}^0p(q,L)$ relate to the base and the end-effector of the soft robot, respectively. Please note that left-sided superscript are used to indicate the frame of reference. The set of all points on the backbone $\mathcal{P}=\left\{{}^0p\in\mathbb{R}^3\mid\sigma\in\mathbb{X}\right\}$ draws a possible spatial configuration of the soft robot given a time instance $t\in\mathbb{T}$ on a finite horizon $\mathbb{T}=[0,T]$.

Intermezzo 1. Despite the inherent flexibility in soft robotics, it is sometimes sufficient to express the kinematics according to the Piecewise Constant Curvature (PCC) condition. Mathematically, it implies that the curvature of the continuous body satisfies $\kappa(q,\sigma_1) = \kappa(q,\sigma_2)$ for a neighboring region of points $\sigma_1,\sigma_2 \subseteq \mathbb{X}$. As a result, this condition allows us to describe the full forward kinematics with a significantly reduced set of generalized coordinates, mitigating kinematic complexity in the model. Numerous works employ PCC models [?,?,?,?,?,?], and depending on the degrees of elasticity, the PCC condition has been proven to be consistent for various soft robotic systems.

Following this Piecewise Constant Curvature (PCC) description, let us assign a coordinate frame that twists minimally along the backbone – a Bishop frame [?]– parametrized by the following generalized coordinate vector:

$$\mathbf{q} = \begin{pmatrix} \varepsilon & \kappa_x & \kappa_y \end{pmatrix}^\top \in \mathcal{Q},\tag{1.4}$$

where $\varepsilon \in \mathbb{R}$ is the elongation strain, and κ_x , $\kappa_y \in \mathbb{R}$ are the curvatures or angular strains in x-z and y-z plane, respectively; and $\mathcal{Q} \subset \mathbb{R}^3$ is an admissible space on which q evolves.It is worth mentioning that the joint description above is somewhat related to Renda. et al. [?] who proposed a Piece-wise Constant Strain (PCS) parametrization with the exception of including the twist along the tangent.

By exploring the differential geometry of the smooth backbone curve similar to Mochiyama et al. [?], we can express the spatial change of the position vector ${}^{0}p(0,q)$ and the orientation matrix ${}^{0}\Phi(q,\sigma)$ for each material point σ along the smooth backbone by

$$\frac{\partial^{0} \Phi}{\partial \sigma} (\sigma, \mathbf{q}) = {}^{0} \Phi(\sigma, \mathbf{q}) \left[\mathbf{\Gamma}(\sigma, \mathbf{q}) \right]_{\times}, \tag{1.5}$$

$$\frac{\partial^{0} \mathbf{p}}{\partial \sigma}(\sigma, \mathbf{q}) = {}^{0} \mathbf{\Phi}(\mathbf{q}, \sigma) \mathbf{U}(\sigma, \mathbf{q}), \tag{1.6}$$

where $[\Gamma]_{\times} \in \text{so}(3)$ is a skew-symmetric matrix composed of the entries of the vector $\Gamma \in \mathbb{R}^3$, and $U \in \mathbb{R}^3$ a vector representing the tangent along the extensible backbone. The vectors Γ and U are vectors that define the differential geometry of the backbone, which are unique entries that lives in the tangent space of the rigid-body transformation group SE(3). Given the Bishop parametrization as described by (1.4), these geometric entities yield

$$\Gamma = \begin{pmatrix} -\kappa_y \\ \kappa_x \\ 0 \end{pmatrix}; \qquad U = \begin{pmatrix} 0 \\ 0 \\ \varepsilon \end{pmatrix} + U_0, \qquad (1.7)$$

with $U_0 = (0,0,1)^{\top}$ the unit-tangent. Now, given an initial configuration of backbone's base, i.e., ${}^0\Phi(0,q) = \Phi_0$ and ${}^0p(0,q) = 0_3$, we can now solve for the position and orientation for each material coordinate σ along the backbone:

$${}^{0}\mathbf{\Phi}(\sigma, \mathbf{q}) = \mathbf{\Phi}_{0} \exp(\sigma[\mathbf{\Gamma}(\mathbf{q})]_{\times}), \tag{1.8}$$

$${}^{0}\boldsymbol{p}(\sigma,\boldsymbol{q}) = \int_{0}^{\sigma} {}^{0}\boldsymbol{\Phi}(\eta,\boldsymbol{q}) \boldsymbol{U}(\boldsymbol{q}) d\eta, \qquad (1.9)$$

where exp : so(3) \rightarrow SO(3) is the exponential map. Let it be clear that the closed-form solutions (1.8) and (1.9) form the forward configuration kinematics of the backbone curve. To express the forward velocity kinematic, let $V(\sigma, q, \dot{q}) = \begin{pmatrix} \sigma \omega^{\top}, \sigma v^{\top} \end{pmatrix}^{\top} \in \mathbb{R}^6 \cong \text{se}(3)$ be the aggregate of the angular velocity and linear velocity components relative to an inertial frame at σ (the frame of reference is denoted by a left superscript), where the space se(3) denotes the Lie algebra of SE(3). The velocity twist is computed by the following integration procedure:

$$V(\sigma, \mathbf{q}, \dot{\mathbf{q}}) = \operatorname{Ad}_{\mathbf{g}(\sigma, \cdot)}^{-1} \int_{0}^{\sigma} \operatorname{Ad}_{\mathbf{g}(\eta, \cdot)} J^{*} \dot{q} \, d\eta =: J(q, \sigma) \dot{q}, \tag{1.10}$$

where $\mathrm{Ad}_g:\mathrm{SE}(3)\to\mathbb{R}^{6\times 6}$ denotes the adjoint transformation matrix regarding the rigid body transformation $g\in\mathrm{SE}(3)$ that maps local velocities (i.e., twist) to a frame located at σ , and J^* a constant joint-axis matrix. The joint-axis matrix for an extensible and bendable PCC segment parametrized by the Bishop parameters is given by

$$J^* := \left(\frac{\partial \Gamma}{\partial q}^{\top} \frac{\partial U}{\partial q}^{\top}\right)^{\top} = \begin{pmatrix} 0 & 0 & 0 & 0 & 1\\ 0 & 1 & 0 & 0 & 0\\ -1 & 0 & 0 & 0 & 0 \end{pmatrix}^{\top}.$$
 (1.11)

Although we based the forward kinematics on the work of Mochiyama et al. [?], the derived expression for the velocity twist in (1.10) is analogous to the work

of Renda et al. [?,?], and Boyer et al. [?,?]. Please also note that (1.10) gives rise to the geometric manipulator Jacobian $J(q,\sigma)$ that defines the mapping from joint velocities to the velocity twist for a particular material point σ on the continuous body. In continuation, let us also introduce the acceleration twist [?,?,?] – obtained through time differentiation of (1.10):

$$\dot{V}(q,\dot{q},\ddot{q},\sigma) = J\ddot{q} + \operatorname{Ad}_{g(\cdot,\sigma)}^{-1} \int_{0}^{\sigma} \operatorname{Ad}_{g(\cdot,\eta)} \operatorname{ad}_{V(\cdot,\eta)} J^{*}\dot{q} \, d\eta$$

$$:= J(q,\sigma)\ddot{q} + \dot{J}(q,\dot{q},\sigma)\dot{q}, \tag{1.12}$$

where $ad_V \in \mathbb{R}^{6 \times 6}$ denotes the adjoint transformation regarding the velocity twist $V \in se(3)$. The reader is referred to Appendix A for more detailed expressions on the adjoint transformations.

1.2.2 Euler-Lagrange equations

Given the forward kinematics in (1.8), (1.9), (1.10) and (1.12), we can shift our attention to formulating the finite-dimensional dynamics of the soft robot. Our goal here is to write the spatio-temporal dynamics of the hyper-elastic soft robot as a second-order ODE into the Lagrangian form:

$$\frac{d}{dt} \left(\frac{\partial \mathcal{L}}{\partial \dot{q}} \right) - \frac{\partial \mathcal{L}}{\partial q} = Q^{\text{nc}}, \tag{1.13}$$

where $\mathcal{L}(q,\dot{q}) := \mathcal{T}(q,\dot{q}) - \mathcal{U}(q)$ is the Lagrangian function, $\mathcal{T} \in \mathbb{R}_{\geq 0}$ and $\mathcal{U} \in \mathbb{R}$ the kinetic and potential energy, respectively; and $Q^{\mathrm{nc}} \in \mathbb{R}^n$ a vector of generalized non-conservative forces. To apply the Lagrangian formalism to a continuum dynamical system, regard an infinitesimal slice of the continuum body for each material coordinate σ along the backbone curve. Given this notion, we embody this infinitesimal slice with an inertia tensor $\mathcal{M} = \mathrm{blkdiag}(\rho I_3, \mathcal{J}_{\sigma})$ with $\rho = m/L$ the line-density and J_{σ} a tensor for the second moment of inertia. The kinetic energy can be obtained through spatial integration of its respective kinetic energy densities [?,?,?], i.e., $\mathfrak{T} = \frac{1}{2}V^{\top}\mathcal{M}V$:

$$\mathcal{T}(q, \dot{q}) = \frac{1}{2} \int_{\mathbb{X}} V(q, \dot{q}, \sigma)^{\top} \mathcal{M} V(q, \dot{q}, \sigma) d\sigma,$$

$$= \frac{1}{2} \dot{q}^{\top} \int_{\mathbb{X}} J(q, \sigma)^{\top} \mathcal{M} J(q, \sigma) d\sigma \dot{q},$$

$$= \frac{1}{2} \dot{q}^{\top} M(q) \dot{q}.$$
(1.14)

Note that expression for the kinetic energy naturally gives rise to the generalized inertia matrix M(q) of the Lagrangian model. By substitution of the kinetic energy into the Euler-Lagrange equation (1.13), we find $M(q)\ddot{q} + C(q,\dot{q})q$

where $C(q, \dot{q})$ denotes the Coriolis matrix. Instead of computing the Coriolis matrix through the conventional Christoffel symbols [?], we adopt a computational scheme by Garofalo et al. [?] used for serial-chain rigid manipulators, in which we replaced the finite summation of N rigid-bodies by a spatial integration over the continuum domain X:

$$C(q, \dot{q}) = \int_{\mathbb{X}} J(q, \sigma)_{V(q, \dot{q}, \sigma)}^{\top} J(q, \sigma) + J(q, \sigma)^{\top} \mathcal{M} \dot{J}(q, \dot{q}, \sigma) \, d\sigma, \quad (1.15)$$

where $C_V = -C_V^{\top} := \mathcal{M} \operatorname{ad}_V - \operatorname{ad}_V^{\top} \mathcal{M}$ is a skew-symmetric matrix. The computation above is slight different from existing literature [?, ?] to ensure that the matrix $\dot{M} - 2C$ is skew-symmetric; the so-called the passivity condition [?] for Euler-Lagrange systems (see Appendix B for proof). The importance of this property will become apparent later in the energy-based controller design. Lastly, the potential energy is given by sum of gravitational potential energy and internal elastic potential, i.e., $\mathcal{U}(q) = \mathcal{U}_g(q) + \mathcal{U}_e(q)$. Since gravitational potential energy density is given by $\mathfrak{U}_g = -\rho^0 p(q, \sigma) \gamma_g$ with $\gamma_g \in \mathbb{R}^3$ is a vector of body accelerations, the potential energy related to gravity is obtained by spatial integration of their respective energy densities:

$$\mathcal{U}_g(q) = -\rho \int_{\mathbb{X}} {}^{0} p(q, \sigma)^{\top} \gamma_g \ d\sigma. \tag{1.16}$$

To model the hyper-elastic nature, lets introduce two nonlinear stiffness functions for both stretching and bending, denoted by $k_e: \mathbb{R} \mapsto \mathbb{R}_{>0}$ and $k_b: \mathbb{R} \mapsto \mathbb{R}_{>0}$, respectively. These functions allow us to describe a collective elastic behavior imposed by the hyper-elastic materials and the continuum-bodied deformation. It shall be clear that these entities are unique to the soft robot's geometry and soft material choice, and thus finding a suitable candidate model requires further analysis. Later, we will sculpt these nonlinear stiffness functions through Finite Element Methods (FEM). For now, we assume that these analytical nonlinear stiffness functions are known, and thus the (hyper)-elastic potential energy takes the form

$$\mathcal{U}_e(q) = \int_0^\varepsilon k_e(\eta) \, \eta \, d\eta + \int_0^{\beta(q)} k_b(\eta) \, \eta \, d\eta, \tag{1.17}$$

where ε is the elongation strain, and $\beta(q) = \kappa L(\varepsilon + 1)$ is the bending angle with the total curvature of the soft segment $\kappa = \sqrt{\kappa_x^2 + \kappa_y^2}$ (see Figure ??).

Overall dynamics

Finally, by combining (1.13), (1.14), (1.15), (1.16), and (1.17), the continuum dynamics of the soft robot can be casted into the familiar closed form [?,?,?,?]

similar to aforementioned model (1):

$$M(q)\ddot{q} + C(q,\dot{q})\dot{q} + P(q,\dot{q}) + G(q) = \tau(u,\delta),$$
 (1.18)

where $P = d\mathcal{U}_e/dq + R\dot{q}$ is a vector of generalized forces imposed by the deformation of the soft materials with $R \in \mathbb{R}^{n \times n}$ the Rayleigh damping matrix, $G = \partial \mathcal{U}_g/\partial q$ a vector of generalized gravitational forces, and $u \in \mathbb{R}^m$ the control input with the index m the number of pressure inputs. The generalized input vector is chosen of the form: $\tau(u, \delta) = Hu + \delta$ with $H : \mathbb{R}^m \to \mathbb{R}^n$ a mapping from the input space to the joint actuation space, and $\delta(t)$ an external disturbance (e.g., unmodelled material uncertainties).

Remark 1. Given the context of manipulators, a possible disturbance $\delta(t)$ could be an external mass applied to the tip of the soft robot. Given the kinematic relations in (1.10) and (1.12), one can describe the disturbance (modeled here as a point-mass located at L) by a state-dependent vector:

$$\delta_m = m_{\delta} \lfloor J(\cdot, L) \rfloor_3^{\top} \left(\operatorname{Ad}_{g(\cdot, L)}^{-1} \gamma_g + \lfloor \dot{V}(\cdot, L) \rfloor_3 \right), \tag{1.19}$$

where $\lfloor \cdot \rfloor_3$ extracts the last three rows of a matrix or vector, and $m_\delta > 0$ the applied mass to the end-effector. It is worth recalling that the acceleration twist can be computed through the geometric Jacobian and its time derivative, i.e., $\dot{V} = J\ddot{q} + \dot{J}\dot{q}$. Indeed, the PCC condition for a soft body can only accurately describe the true dynamics if external forces produced by mass m_δ do not excessively exceed the intrinsic elastic balancing forces P(q). Alternatively, a soft body can be modeled using multiple PCC curves of smaller size, similar to standard Finite Element discretization.

The actuation mapping H depends on the geometry, placement, and orientation of the (pneumatic) soft actuators. Since the pneumatic chambers are aligned parallel to the backbone curve and are equally spaced along the circumference, we propose the following ansatz:

$$H := \begin{pmatrix} \alpha_{\varepsilon} & \dots & \alpha_{\varepsilon} \\ -\alpha_{\kappa} \cos(\phi_{1}) & \dots & -\alpha_{\kappa} \cos(\phi_{m}) \\ \alpha_{\kappa} \sin(\phi_{1}) & \dots & \alpha_{\kappa} \sin(\phi_{m}) \end{pmatrix}, \tag{1.20}$$

where $\alpha_{\varepsilon}, \alpha_{\kappa} > 0$ are system parameters representing the effective transferal of differential pressure to joint forces, and $\phi_i = (i-1) \cdot \frac{2\pi}{m}$ the angular inter-distance between the m-number of pneumatic bellows. Please note that the parameters α_{ε} and α_{κ} are dependent on the bellow area and radius from the bellow to the backbone curve.

1.3 Extension to multi-link dynamics

We previously expressed the position and velocity kinematics as explicit functions of the generalized coordinates (i.e., Bishop parameters) and their time-derivatives. This explicit dependency stems from the PCC conditions inferring the curvature is non-varying along the spatial domain \mathbb{X} , i.e., $\kappa(q,\sigma) = \kappa(q)$. Although sufficient for some cases, the condition is generally restrictive, and to some extent inconvenient, since the inclusion of multiple links demands piecewise integration of the kinematics (1.9), (1.8), (1.10), and (1.12). Rather than separation of integration, we can extend this PCC description by using piece-wise continuous spatial function to distinguishes multiple soft-bodied links along the continuous body of the soft robot. The idea of parametrization through shapes functions has been explored earlier by Chirikjian et al. [?,?], and later by Boyer et al. [?], Della Santina et al. [?]. A similar discontinuous shape function series was used by Berthet-Rayne et al. [?] to pursue multi-body dynamics for growing continuum robots; and proposed by Chirikjian [?] for hyper-redundant robots earlier.

Following the aforementioned works, let us parameterize the the geometric vectors Γ and U for a N-link soft robot through the product of a basis of orthonormal functions $\{s_i\}_{i\in\mathbb{N}}$ and the Bishop parametrization as follows

$$\Gamma(q,\sigma) = \sum_{i=1}^{N} s_i(\sigma) \lceil J^* \rceil_3 \,\tilde{q}_i, \tag{1.21}$$

$$U(q,\sigma) = \sum_{i=1}^{N} s_i(\sigma) \lfloor J^* \rfloor_3 \, \tilde{q}_i + U_0, \qquad (1.22)$$

where J^* is the joint-axis matrix as in $(\ref{eq:condition})$, the mathematical operators $\lceil \cdot \rceil_3$ and $\lfloor \cdot \rfloor_3$ extract the first or last three rows of a matrix, respectively; \tilde{q}_i the joint variables of the i-th link, and $s_i : \mathbb{X} \mapsto \{0,1\}$ is a piece-wise continuous shape function, whose purpose is to be non-zero for a given interval on \mathbb{X} . The new generalized coordinate vector becomes the aggregate of all joint variables of the multi-body soft robotic system $q = (\tilde{q}_1^\top, \tilde{q}_2^\top, ..., \tilde{q}_N^\top)^\top$ with the vector $\tilde{q}_i = (\varepsilon_i, \kappa_{x,i}, \kappa_{y,i})^\top$ relating to the Bishop parametrization of the ith-link. Given (1.21) and (1.22), we may now rewrite the velocity-twist as

$$V(q, \dot{q}, \sigma) = \operatorname{Ad}_g^{-1} \int_0^{\sigma} \operatorname{Ad}_g J^* S(\sigma) \, d\sigma \dot{q} := J(q, \sigma) \dot{q}$$
 (1.23)

where $S=(s_1,\,s_2,\,...,s_N)\otimes I_n$ is an unitary selection matrix derived from the basis of piece-wise continuous shape functions $\{s_i\}_{i=1}^N$. To be less ambiguous about this selection matrix S, lets consider a spatial coordinate $\sigma_2\in [L_1,L_1+L_2]$ that lies on the spatial interval of the second link. Consequently, the operation $S(\sigma_2)q=\tilde{q}_2$ returns the corresponding joint variable of the second link. This

selection of generalized coordinates follows analogously for other links along the serial-chain of the soft manipulator. We provided a small library of piece-wise continuous shape functions upto $1 \le N \le 8$ links under ./src/pwf on the open repository [?]. Now, substitution of the discontinuous variation of the geometric Jacobian in (1.23) into (1.14) leads to the dynamic model of a N-link soft robot manipulator in the Lagrangian form similar to (1.18).

1.4 Efficient computation of the continuum dynamics

Due to the partial differential nature of soft robots, obtaining a closed-form expression for the projected Lagrangian model in (1.18) can become notoriously long and complex (especially for multi-link systems). The origin of this problem stems from the integrands of inertia matrix M(q) in (1.14) and Coriolis forces $C(q, \dot{q})$ in (1.15); which become highly nonlinear and therefore difficult to calculate a-priori. As a result, solving the forward dynamics using traditional solvers often deteriorates the real-time performance, and in turn its usability for closed-loop control. Inspired by Boyer et al. [?] and Godage et al [?], instead of finding an exact solution to the dynamic entries M(q), $C(q, \dot{q})$ and G(q), let us introduce a similar reduced-order integration scheme that produces an approximate of the dynamic model (1.18). Yet, instead of using an inverse Newton-Euler algorithm (i.e., Featherstone or Hollerbach scheme) in which the Lagrangian entries are built column-wise, we propose an explicit integration scheme that efficiently computes all Lagrangian entities in parallel through a so-called Matrix-Differential Equation (MDE).

The idea here is to replace all necessary spatial integrations for the computation of the Lagrangian entities by an equivalent Matrix-Differential Equation of the form:

$$\frac{\partial Z}{\partial \sigma} = F(Z, \sigma), \tag{1.24}$$

where $Z(\cdot, \sigma)$ is a matrix-valued function composed of the necessary elements for the forward kinematics and forward dynamics, and $F(Z, \sigma)$ a matrix-valued flow function that describes the spatial evolution of Z. Then, by choosing the appropriate initial condition for $Z(\cdot, 0) = Z_0$ and numerically solving (1.24) over a finite horizon \mathbb{X} , we can retrieve an approximate of the Lagrangian model in (1.18) by extracting the necessary elements from the solution $Z(\cdot, L)$.

Before describing the MDE, let us first introduce two intermediate matrices related to the computation of the manipulator Jacobian and its time-derivative, namely:

$$\frac{\partial B_1}{\partial \sigma} = \operatorname{Ad}_{g(\cdot,\sigma)} J^* S(\sigma), \tag{1.25}$$

$$\frac{\partial B_2}{\partial \sigma} = \operatorname{Ad}_{g(\cdot,\sigma)} \operatorname{ad}_{V(\cdot,\sigma)} J^* S(\sigma)$$
(1.26)

such that they satisfy $J\dot{q} = \mathrm{Ad}_g^{-1}B_1\dot{q}$ and $\dot{J}\dot{q} = \mathrm{Ad}_g^{-1}B_2\dot{q}$. Given the expressions above, we can now include a partial computation Jacobians into the MDE. By collecting all the differential relation for the forward kinematics (5), (6) and forward dynamics (14), (15), and (16), we can assign a flow function $F := \mathrm{blkdiag}(F_1, F_2)$ composed of two matrices:

$$F_1 = \begin{pmatrix} {}^{0}\Phi[\Gamma]_{\times} & {}^{0}\Phi U \\ 0_{3\times 3} & 0_3 \end{pmatrix} \quad \operatorname{Ad}_g J^* S \quad \middle| \quad \operatorname{Ad}_g \operatorname{ad}_V J^* S \right), \tag{1.27}$$

$$F_2 = \begin{pmatrix} \frac{\partial M}{\partial \sigma} & \frac{\partial C}{\partial \sigma} & \frac{\partial G}{\partial \sigma} \end{pmatrix}, \tag{1.28}$$

in which the differential form of the dynamic entities M(q), $C(q, \dot{q})$, and G(q) of the Lagrangian model are given by

$$\frac{\partial M}{\partial \sigma} = (\mathrm{Ad}_q^{-1} B_1)^{\top} \mathcal{M} (\mathrm{Ad}_q^{-1} B_1), \tag{1.29}$$

$$\frac{\partial C}{\partial \sigma} = (\operatorname{Ad}_g^{-1} B_1)^{\top} \left[\mathcal{C}_V(\operatorname{Ad}_g^{-1} B_1) + \mathcal{M}(\operatorname{Ad}_g^{-1} B_2) \right], \tag{1.30}$$

$$\frac{\partial G}{\partial \sigma} = (\lfloor B_1 \rfloor_3)^{\top} \rho \gamma_g, \tag{1.31}$$

We wish to stress that F_1 collects all elements related to the forward kinematics, whereas F_2 contains the dynamic entities related to the Lagrangian model. Following the spatial Matrix-Differential equation in (1.24) above, its solution will be a matrix $Z := \text{blkdiag}(Z_1, Z_2)$ composed of two smaller state matrices Z_1 and Z_2 :

$$Z_1 := \begin{pmatrix} {}^{0}\Phi & {}^{0}p \\ {}^{0}_{3\times 3} & {}^{0}_{3} \end{pmatrix} B_1 \quad B_2 \quad , \tag{1.32}$$

$$Z_2 := \begin{pmatrix} M & C & G \end{pmatrix}, \tag{1.33}$$

Such a Matrix-Differential equation as in (1.24) are not supported natively by standard ODE solvers. Therefore, an explicit second-order Runge-Kutta solver for MDEs is developed such that efficiently computes the evolution of the state matrix Z along X. The solver is written in MATLAB and can be found under ./src/Model.m at Caasenbrood [?].

As for state trajectories along the temporal regime $\mathbb{T}=[0,T]$, an implicit trapezoidal integration scheme is proposed to solve the approximated continuum dynamics, which are generally less conservative on discretization to preserve numerical stability. Here implicit schemes are favored over explicit scheme, since a coarser time integration can significantly increase real-time performance. In addition, to further boost performance of the temporal integration, a cost-effective approximation of the Hessian is introduced. For more detail, see Appendix C for more detail.